Microfluid Nanofluid (2016) 20:150
DOI 10.1007/s10404-016-1815-1

RESEARCH PAPER

Numerical investigation of micro- and nanochannel deformation due to discontinuous electroosmotic flow

Joseph M. de Rutte[1] · Kjeld G. H. Janssen[1] · Niels R. Tas[2] · Jan C. T. Eijkel[2] · Sumita Pennathur[1]

Received: 17 June 2016 / Accepted: 11 October 2016 / Published online: 20 October 2016
© Springer-Verlag Berlin Heidelberg 2016

Abstract Large pressures can induce detrimental deformation in micro- and nanofluidic channels. Although this has been extensively studied for systems driven by pressure and/or capillary forces, deflection in electrokinetic systems due to internal pressure gradients caused by non-uniform electric fields has not been widely explored. For example, applying an axial electric field in a channel with a step change in conductivity and/or surface charge can lead to internally generated pressures large enough to cause cavitation, debonding, and/or channel collapse. Finite electric double layers within nanofluidic channels can further complicate the physics involved in the deformation process. In order to design devices and experimental procedures that avoid issues resulting from such deformation, it is imperative to be able to predict deformation for given system parameters. In this work, we numerically investigate pressures resulting from a step change in conductivity and/or surface charge in micro- and nanofluidic channels with both thin and thick double layers. We show an explicit relation of pressure dependence on concentration ratio and electric double layer thickness. Furthermore, we develop a numerical model to predict deformation in such systems and use the model to unearth trends in deformation for various electric double layer thicknesses and both glass and PDMS on glass channels. Our work is particularly impactful for the development and design of micro- and nanofluidic-based devices with gradients in surface charge and/or conductivity, fundamental study of electrokinetic-based cavitation, and other systems that exploit non-uniform electric fields.

Keywords Electrokinetic · Microfluidics · Nanofluidics · Deformation

1 Introduction

Deformation in micro- and nanofluidic channels has become an important consideration with the increasing use of elastomers and other flexible materials, as well as the resulting higher pressures needed in Lab-on-chip (LOC) applications due to increasing incorporation of nanoscale features (Xia and Whitesides 1998; Quake and Scherer 2000; Abgrall and Nguyen 2008). Specifically, deformation is often associated with high local pressures which can complicate measurements and even cause failure in micro- and nanofluidic channels. For example, expansion in microchannels may lead to larger flow rates and cause unwanted capacitive effects (Dendukuri et al. 2007). In the case of extremely large pressures, channel geometries can debond (due to high positive pressures) (Pennathur 2001), or collapse (due to high negative pressures). Although there are such adverse effects associated with microchannel deformation, there have also been several studies in which deformation has been exploited (Unger et al. 2000; Hosokawa et al. 2001). For example, Unger et al. fabricated complex systems of active pumps and valves exploiting deformation, and Hosokawa et al. used deformable PDMS

Electronic supplementary material The online version of this article (doi:10.1007/s10404-016-1815-1) contains supplementary material, which is available to authorized users.

✉ Sumita Pennathur
sumita@engineering.ucsb.edu

[1] Department of Mechanical Engineering, University of California, Santa Barbara, Engineering Science Building, Room 3231C, Santa Barbara, CA, USA

[2] MESA+ Institute for Nanotechnology, University of Twente, P.O. Box 217, 7500 AE Enschede, The Netherlands

diffraction grating for local pressure sensing. In either case, deformation is an important consideration in designing micro- and nanoscale systems, especially when using soft materials and/or nanoscale structures.

Furthermore, there have been many studies regarding the deformation process itself. For example, Gervais et al. experimentally measured deformation due to pressure-driven flow in PDMS microchannels of various sizes and elastic moduli using confocal microscopy and validated their work using both analytical and numerical simulations. Hardy et al. (2009) expanded on this work by studying the dependence of substrate thickness on resulting deformation using fluorescent microscopy. Other researchers have studied deformation due to capillary driven flow (van Honschoten et al. 2007; Majumder et al. 2010). For example, van Honschoten et al. studied the effect of deformation on capillary filling rates of various sized nanofluidic channels in silicon, and Majumder et al. studied capillary-filling-based deformation of circular cross-sectional microchannels in PDMS.

Despite the plethora of both experimental and theoretical micro- and nanochannel deformation literature, there is a dearth of literature investigating deformation within electrokinetic flow systems, where large induced pressures have been demonstrated (Herr et al. 2000; Bharadwaj and Santiago 2005; Lenzi et al. 2011; Janssen et al. 2011). Furthermore, with the increasing ability to microfabricate nanoscale features (Mijatovic et al. 2005), and use of electrokinetics (Bruin 2000), understanding and/or predicting deformation is essential to the design and development of robust electrokinetic devices. For example, deformation can not only change hydraulic resistance and therefore resulting flow profiles, but can also affect analyte separation, concentration, and dispersion behavior in electrokinetic systems with non-uniform conductivity and/or surface charge distribution. These discontinuities are commonly utilized in preconcentration and separation techniques such as isotachophoresis (ITP) (Wainright et al. 2002) and field amplified sample stacking (FASS) (Bharadwaj and Santiago 2005), as well as observed in novel phenomena such as electrocavitation (Janssen et al. 2011; Janssen and Pennathur 2015). For example, pressures of −1320 bar have been reported in nanofluidic electrocavitation systems (van Schoot et al. 2014), large enough to cause deleterious deformation.

In this paper, we numerically investigate deformation in typical electrokinetic micro- and nanofluidic systems. Specifically, we examine the pressures and resulting deformation that can be induced in electrokinetic systems with a step change in both conductivity and ζ-potential, as shown in Fig. 1. We first derive an analytical model for pressures that can be induced in thin EDL systems in order to understand general trends and validate our numerical model. We

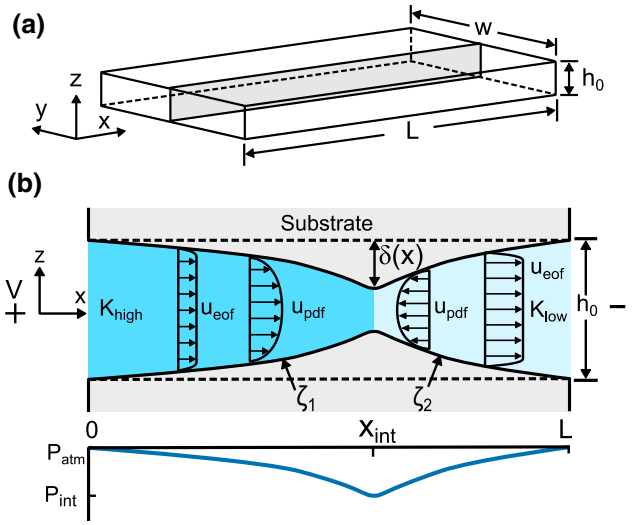

Fig. 1 **a** Geometry of the channel where w is channel width, h_0 is channel height, and L is channel length. **b** Schematic of axial deflection during electrokinetic flow through a channel with a step change in conductivity (K) and ζ-potential (ζ) at the interface position X_{int}. A potential V is applied across the channel which creates a non-uniform electric field. The resulting step change in electroosmotic flow velocity (u_{eof}) is balanced by internal pressure gradients and resultant pressure-driven flow velocity (u_{pdf}). The resulting pressure distribution deflects the channel wall by a distance δ that is dependent on the local pressure

then solve numerically using a 2D COMSOL model for thin and thick EDL systems in order to account for nonlinear electric double layer effects, typical of nanofluidic electrokinetic systems. Next, we outline a method to quantify deformation for typical channel geometries and material properties using scaling arguments previously proposed by Gervais et al. (2006). We then couple deformation with our 2D flow model. Because hydraulic resistance is strongly dependent on channel geometry, we outline a solution procedure for coupling the effect between our electrokinetic flow system and deformation. We show relationships that can be used to find the deformation in particular electrokinetic system of interest. To demonstrate this, we report few case examples to estimate maximum deformation and predict system failure.

2 Analytical model (no deformation)

In electrokinetic systems, internal pressure gradients arise with non-uniformities in conductivity, ζ-potential, double layer thickness, permittivity, viscosity, and electric field (Bharadwaj and Santiago 2005; Herr et al. 2000; Lenzi et al. 2011). Among these, the most commonly encountered in typical electroosmotic microfluidic systems are step changes in conductivity and ζ-potential. For example,

step changes in conductivity form the basis of the analyte separation and concentration techniques such as FASS and ITP (Bharadwaj and Santiago 2005; Wainright et al. 2002). Non-uniform ζ-potentials arise due to different surface compositions, either chemical or electrical (Herr et al. 2000; Lenzi et al. 2011; Loessberg-Zahl et al. 2016) Furthermore, since ζ-potential is typically dependent on ion concentration (Hunter 1981), a non-uniform electrolyte concentration can also induce non-uniform ζ-potentials. In order to better understand which parameters are significant in pressure generation as well as to later provide validation for our 2D flow model, we first derive a simple 1D analytical solution for pressure in a channel with a step change in conductivity and ζ-potential.

2.1 Model geometry

We consider a rectangular channel of height h_0, width w, and length L with a step change in both conductivity (K_{high} to K_{low}) and ζ-potential (ζ_1 to ζ_2) at some interface position X_{int} (Fig. 1). For simplicity, we assume that $h \ll w$, a reasonable approximation for typical micro-/nanofluidic systems (Squires and Quake 2005). A potential difference V is applied axially across the channel generating non-uniform electroosmotic flow (EOF) which is balanced by induced pressure gradients within the channel. For significantly large pressures, the channel wall will deflect some distance δ.

2.2 Governing equations

For typical micro-/nanofluidic systems, the Reynolds number is sufficiently low such that the fluid flow can be described by the incompressible Stokes equations with an electrokinetic body force (Squires and Quake 2005):

$$0 = \nabla \cdot \boldsymbol{u} \tag{1}$$

$$0 = -\nabla p + \nabla \cdot \left(\frac{\mu}{\rho}\nabla \boldsymbol{u}\right) - \epsilon \boldsymbol{E}\nabla^2\psi$$

where $\boldsymbol{u}$ is the fluid velocity vector, p is pressure, μ is dynamic viscosity, ρ is density, ε is permittivity, $\boldsymbol{E}$ is the axial electric field, and ψ is the electric potential in the electrical double layer. Here, we consider an equilibrium system such that the potential distribution across the channel can be described by the Poisson–Boltzmann equation

$$\nabla^2\psi = -\frac{e}{\epsilon}\sum_{i=1}^{N} Z_i n_{\infty,i} \exp\left(-\frac{Z_i e\psi}{k_{\text{B}}T}\right) \tag{2}$$

where i indicates the i'th ion type in solution, Z is ion valence number, n_∞ is number density of ions in bulk solution, e is elementary charge, k_{B} is the Boltzmann constant, and T is temperature. The electric fields in the channel are determined by applying conservation of electric current:

$$\nabla \cdot (K\boldsymbol{E}) = 0 \tag{3}$$

For our analytical model, we assume a symmetric background electrolyte in a channel with thin electric double layers, where we use the Debye–Hückel approximation and define the EDL thickness as (Hunter 1981):

$$\lambda_D = \left(\frac{\epsilon k_{\text{B}}T}{2e^2Z^2n_\infty}\right)^{1/2} \tag{4}$$

In this limit, the electric double layer (EDL) thickness is small compared to the channel height ($\lambda_D/h_0 \ll 1$), and thus the mean EOF velocity (u_{eof}) can be described using the Helmholtz–Smoluchowski equation:

$$u_{\text{eof}} = -\epsilon E_x \zeta/\mu \tag{5}$$

where ζ is the ζ-potential. Furthermore, in the limit that the channel width is much larger than the channel height ($w \gg h$), the mean pressure-driven flow velocity (u_{pdf}) is simply:

$$u_{\text{pdf}} = \frac{h_0^2}{12\mu}\left(\frac{\mathrm{d}p}{\mathrm{d}x}\right) \tag{6}$$

The pressure at the interface position (p_{int}) (see Fig. 1) is determined by applying continuity (Eq. 1) at the interface to find:

$$p_{\text{int}} = \frac{12\epsilon V}{h_0^2 L}(\zeta_2 - \zeta_1 a)\left(\frac{X_{\text{int}}(L - X_{\text{int}})}{X_{\text{int}}(a-1) + L}\right) \tag{7}$$

where V is voltage, X_{int} is the interface position, L is channel length, and a is the conductivity ratio $K_{\text{low}}/K_{\text{high}}$. For this system, the pressure distribution is simply a linear distribution between atmospheric pressure (p_{atm}) and p_{int}. The maximum (minimum) pressure is always located at the interface, but the magnitude of this pressure varies depending on the location of the interface. Because we are mostly interested in the maximum pressure generated (for the purposes of microfluidic design), we calculate the position of the maximum pressure possible for the system as

$$X_{\text{max}} = \frac{L\sqrt{a} - L}{a - 1} \tag{8}$$

for a given conductivity ratio a and channel length L. Combining Eqs. (7, 8) gives the following expressions for the maximum pressure in a given system.

$$p_{\text{max}} = \frac{12\epsilon V}{h_0^2}(\zeta_2 - \zeta_1 a)\left(\frac{-2\sqrt{a} + a + 1}{(a-1)^2}\right) \tag{9}$$

To generalize, we non-dimensionalize the pressure by a characteristic pressure p_c, which is the pressure at a conductivity ratio approaching zero:

$$p_c = \frac{12\epsilon V \zeta_2}{h_0^2}. \tag{10}$$

Note that when the conductivity ratio approaches zero, the electric field, and thus EOF, is dominant in the low-conductivity region. Therefore, the resulting induced pressure is not dependent on the surface charge in the high-conductivity region (ζ_1) and is only dependent on permittivity, applied voltage, channel height, and surface charge of the low-conductivity region (ζ_2).

Non-dimensionalizing Eq. (9) using Eq. (10), we derive the following expression for a non-dimensional pressure $\bar{p}$:

$$\frac{p_{\max}}{p_c} = \bar{p} = \left(1 - \frac{\zeta_1}{\zeta_2} a\right)\left(\frac{-2\sqrt{a} + a + 1}{(a-1)^2}\right). \tag{11}$$

The above expression removes the dependence of voltage, permittivity, and channel height, so we can generalize induced pressure based only on ζ ratio and conductivity ratio.

It should be noted that although the 1D model we describe here does not necessarily describe all of the flow properties for our given system, it provides a good approximation for the pressure in the system for a non-deflected channel.

3 Analytical results (no deformation)

In this section, we will address results for resulting induced pressure in the cases of both step changes in conductivity (concentration) and ζ-potential.

3.1 Pressure due to a step change in conductivity

Here, we consider a single-step change in conductivity at some interface position X_{int} (Fig. 1b). Since the ζ-potential is directly dependent on the local concentration/conductivity in the channel, we first quantify the significance of this dependence. We approximate the ζ-potential dependence on concentration using the following exponential model

$$\zeta = AC^B \tag{12}$$

where C is the concentration of the specific region and A and B are constants that depend on the chemistry of the ionic solution and the surface. Previous researchers have experimentally corroborated this model for constant pH systems, with resulting values of B ranging from -0.2 to -0.3 (Bharadwaj and Santiago 2005; Pennathur and Santiago 2005; Sadr et al. 2004). Since most micro-/nanofluidic devices use buffers as ionic solutions, this is a very reasonable approximation for common systems. In the simplest embodiment of microfluidic preconcentration systems, the same electrolyte is used in both the low- and high-concentration region, and therefore, applying Eq. (12) to Eq. (11) yields

$$\bar{p} = \left(1 - a^{1-B}\right)\left(\frac{-2\sqrt{a} + a + 1}{(a-1)^2}\right) \tag{13}$$

for non-dimensional maximum pressure ($\bar{p}$). Note that with a uniform electrolyte, A does not affect $\bar{p}$. Furthermore, $\bar{p}$ never depends on the magnitude of concentration, only on the concentration/conductivity ratio a and the exponent parameter B.

Figure 2a shows $\bar{p}$ versus conductivity ratio for the case of constant ζ-potential ($B = 0$) as well as for the concentration dependent cases at the limits of the range mentioned above ($B = -0.2$ and $B = -0.3$). In the subplot, we show the interface position where the maximum pressure occurs ($X_{\max}/L$) for a given conductivity ratio. As a goes to zero $X_{\max}/L$ is near the outlet of the low-conductivity region and approaches the center of the channel as a goes to 1. Furthermore, we show that the actual difference in pressure (Fig. 2b) and percent difference (Fig. 2c) are dependent on the conductivity ratio. Interestingly, ζ-potential dependence on concentration has very little effect on the actual pressures generated (Fig. 2a), with $\bar{p}$ increasing a maximum difference of only 0.038 for the most extreme case where $B = -0.3$ (Fig. 2b). Furthermore, ζ-potential dependence on concentration is not important at the high and low ends of conductivity ratio for two different reasons. First, in the limit that the conductivity ratio approaches 1, the concentrations are similar, and therefore, the ζ-potential values in the two regions are approximately equal. Second, in the limit that the conductivity ratio goes to zero, the electric field in the high-conductivity region also goes to zero due to conservation of current. Therefore, the electric field (and thus ζ-potential) in the low-conductivity region is dominant. In either case, since the difference in $\bar{p}$ is generally small (<0.04 in all cases of a) and only depends on one ζ-potential, we may assume a constant ζ-potential that is equal to the ζ-potential in the low-conductivity region (where the electric field will dominate). Although it is not necessarily a good approximation for studying all electrokinetic phenomenon, for the purposes of calculating deformation, in the majority of cases of interest, this approximation will give accurate results.

3.2 Pressure generation due to step change ζ-potential

Discontinuities in ζ-potential are not exclusively due to discontinuities in concentration. For example, we can directly change the ζ-potential through chemical surface modification (Herr et al. 2000) or fabricated integrated electrodes

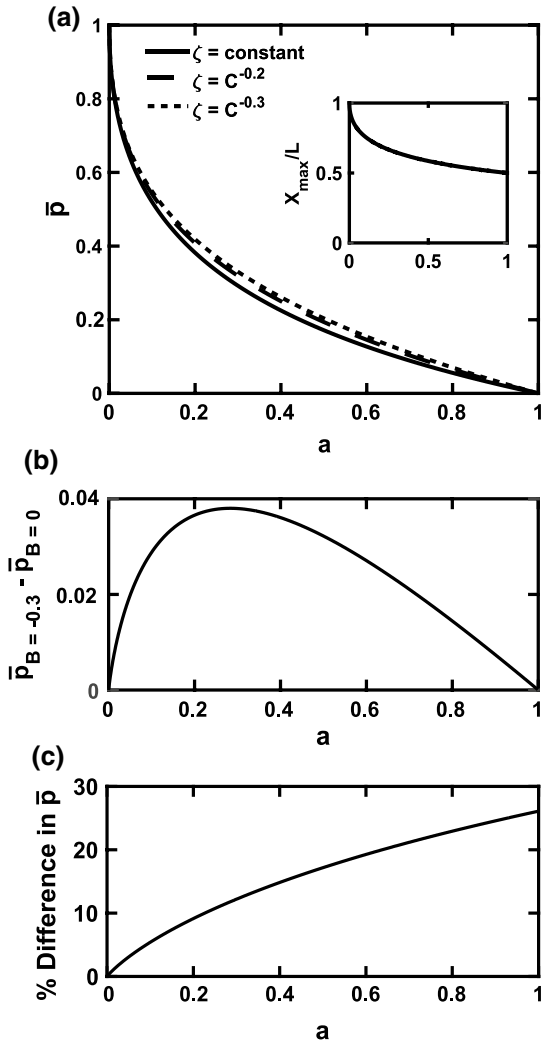

Fig. 2 **a** Non-dimensional maximum pressure ($\bar{p}$) as a function of conductivity ratio for various ζ-concentration relationships. Inset shows relative interface position where maximum pressure occurs for a given conductivity ratio. **b** Relative difference in pressure between the constant ζ-potential solution and $\zeta = C^{-0.3}$ solution. A maximum difference of 0.038 is located at $a = 0.28$. **c** Percent difference as a function of conductivity ratio. As the conductivity ratio approaches zero, the ζ-potential term in Eq. (13) goes to zero and there is no difference between the solutions

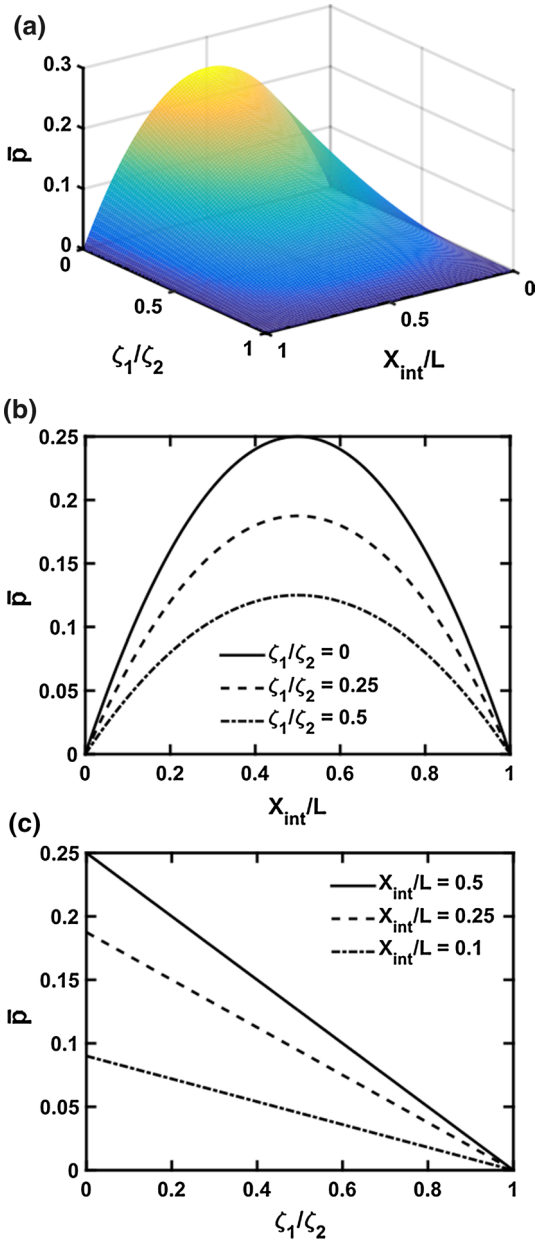

Fig. 3 **a** $\bar{p}$ due to a step change in ζ-potential as a function of ζ-potential ratio ζ_1/ζ_2 and relative interface position X_{int}/L. **b** $\bar{p}$ has a parabolic dependence on the relative interface position, and a **c** linear dependence on ζ_1/ζ_2. As ζ_1/ζ_2 is decreased, the mismatch in EOF between the two regions increases proportionally and $\bar{p}$ increases. $\bar{p}$ has a maximum value of 0.25 at the center of the channel for a ζ-potential ratio of 0

(Lenzi et al. 2011). Considering a step change in ζ-potential at various positions in the channel (X_{int}/L), we examine maximum pressure generated through external modification of ζ-potential. We assign the step change of ζ-potential at a particular location along the channel, unlike systems with non-uniform conductivity gradients, where the system is dynamic. Therefore, from Eq. (7), we can derive the following expression for non-dimensional pressure as a function of relative interface position and ζ-potential ratio, ζ_1/ζ_2 as:

$$\frac{p_{\text{int}}}{p_{\text{c}}} = \bar{p} = \left(1 - \frac{\zeta_1}{\zeta_2}\right)\left(\frac{X_{\text{int}}}{L}\left(1 - \frac{X_{\text{int}}}{L}\right)\right) \tag{14}$$

Figure 3 shows $\bar{p}$ for a range of ζ-potential ratios and all possible interface positions. Both Eq. (14) and Fig. 3 show that $\bar{p}$ has a linear dependence on the ζ-potential ratio and a parabolic dependence on the relative interface position. $\bar{p}$ increases with decreasing ζ-potential ratios because larger differences between ζ-potentials cause larger differences in EOF, and thus larger pressures. We also note that $\bar{p}$ is

minimized when the interface is at the inlet or outlet, and $\bar{p}$ is maximized at the center of the channel. Interestingly, these results demonstrate that the magnitude of pressures generated from a step change in ζ-potential can be comparable to those generated due to conductivity alone ($\bar{p} = 1$ vs. $\bar{p} = 0.25$). Although the effects of concentration dependent ζ-potential are expected to be minimal, large differences in ζ-potential due to non-uniform surface properties can be significant and should not be ignored.

These results give insight into induced pressure due to step changes in properties of electrokinetic systems, but they only specifically address two limiting cases: (1) that of a step change in one electrolyte of similar conductivity and (2) a step change in ζ-potential, using the same electrolyte system. In many systems, two or more different ionic solutions may be used. In this case, the ζ-potential dependence on concentration will be different depending on the solution and will either exacerbate or reduce the induced pressure. Although we do not address it here, it is straightforward to calculate the pressure induced with electrolytes of dissimilar composition using Eq. (11) and specifying the ζ-potential calculated for each region. Similarly, difference in viscosity and electric fields can be accounted for by using Eqs. (5, 6) and applying continuity. If larger ions are used, and/or there are charge inversion effects that may exacerbate the induced pressures, other computational methods such as density functional theory or modified Carnahan–Sterling may be used (Gillespie 2015).

4 Numerical model

Our analytical model can accurately describe generated pressures in simple systems with step changes in conductivity and/or ζ-potential in microchannel systems with thin EDLs. However, with the recent experimental discovery of electrocavitation in nanofluidic systems (Janssen et al. 2011), thick EDLs must be explored. Furthermore, pressures generated will induce a deformation, which in turn will affect the hydrodynamics of systems, so an iterative solving scheme must be used. Therefore, we developed a COMSOL model to account for both thick EDLs and determine iterative deformation solutions.

4.1 Flow model

4.1.1 Solution methodology

The governing equations for potential distribution, electric fields, and resulting fluid flow and pressure distribution are solved using finite element analysis employing COMSOL v4.4 (Comsol, Inc., Stockholm, Se). A segregated solver is used to iteratively solve the incompressible Stokes flow, Poisson–Boltzmann, and conservation of electric currents equations (Eqs. 1, 2, 3, respectively).

In order to quantify the effects of EDL thickness, we define the thickness to be the Debye length λ_D (Eq. 4) as in our analytical model. Since the λ_D will be dependent on the local concentration, we will refer to the relative EDL thickness as the ratio between λ_D and channel height in the region of lowest concentration (largest relative EDL thickness).

4.1.2 Boundary conditions

Three domains are defined, a low-conductivity region, high-conductivity region, and an interface region. We use a second-order continuous step function for the step change in conductivity (concentration) in the finite interface region. The boundary conditions for Poisson–Boltzmann, conservation of electric current, and Navier–Stokes equations are as follows:

$$\psi_{\text{wall}} = \zeta, n \cdot (\nabla\psi)_{\text{wall}} = 0; \tag{15}$$

$$n \cdot (K\boldsymbol{E})_{\text{wall}} = 0, V_{\text{inlet}} = V, V_{\text{outlet}} = 0 \tag{16}$$

$$\boldsymbol{u}_{\text{wall}} = 0, p_{\text{inlet, outlet}} = \left(\mu\nabla^2\boldsymbol{u}\right)\boldsymbol{n}_{\text{inlet, outlet}} = 0 \tag{17}$$

The surface potential is defined by a constant ζ-potential in the low-conductivity region (typically −25 mV). Note that our constant ζ-potential assumption is further validated by our numerical model, which compares constant and concentration dependent ζ-potential for our cases of interest (see supplementary information, S4). For electric field calculations, we assume a bulk conductivity throughout the channel and perfectly insulating walls (Eq. 16). When solving the Stokes flow equation, we apply a zero stress boundary condition on the inlets and outlets and a no slip condition at the channel wall (Eq. 17).

4.1.3 Meshing

Linear quadrilateral elements were used for all meshing. A higher mesh density was implemented near the walls and the interface region to account for the large potential gradients in these regions. In order to reduce the total number of elements, a geometric sequence was used away from both the wall and interface regions, with elements increasing in size. The element ratio of the geometric sequence was increased with decreasing EDL thickness in order to maintain proper mesh density in the EDL region. It was observed that the solution became mesh independent at approximately 18,000 elements (within 1 % of extremely fine mesh solution). The results presented in this work were all obtained using a mesh containing 42,500 elements.

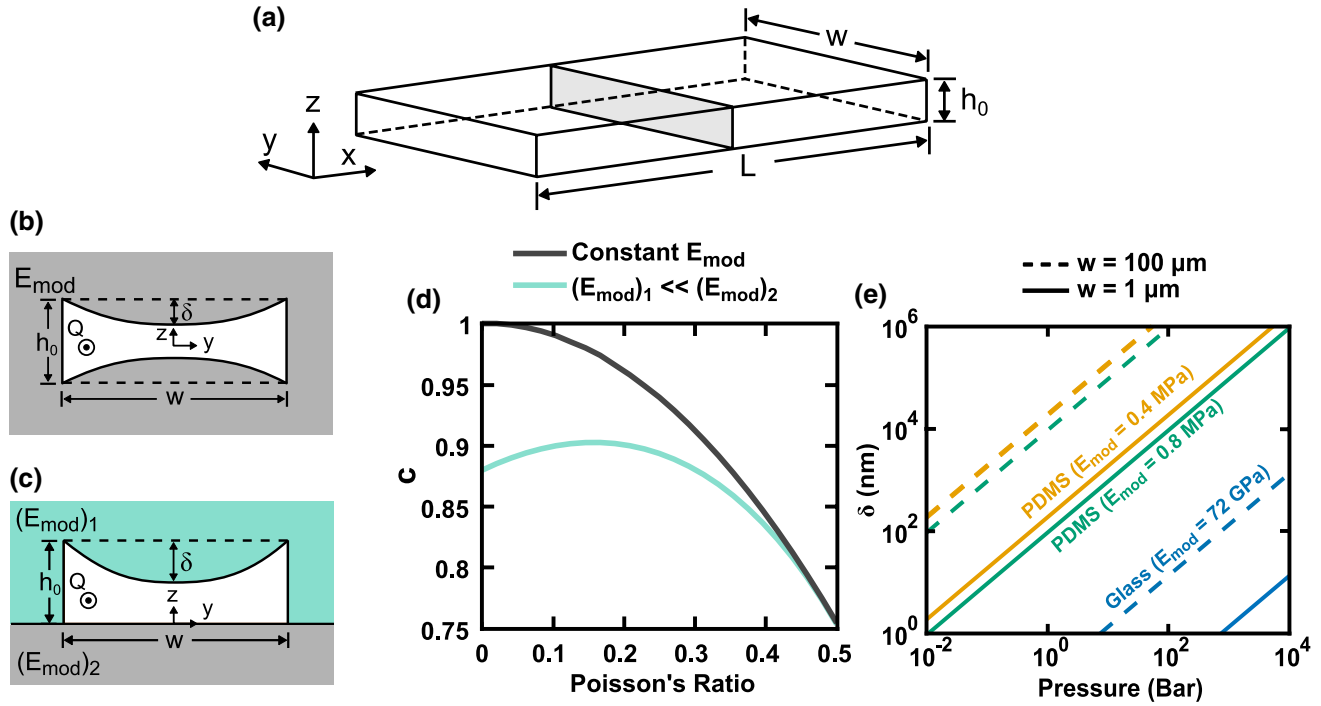

Fig. 4 **a** Channel diagram showing cross section of interest (flow Q is directed along the x-axis). **b** Cross section of a channel in a homogenous material. The *top* and *bottom* walls deflect the same amount δ, given by Eq. (18). **c** Cross section of a microfluidic channel fabricated from a soft material bonded to a relatively stiff material (e.g., PDMS on glass). In this limiting case, only one wall deflects. **d** The proportionality constant c numerically calculated using a 2D structural finite element model. The model shows that c depends only on the Poisson's ratio ν for the geometric conditions described in (**b**, **c**). **e** δ as a function of pressure for typical microfluidic channel widths and materials. $\nu_{\text{PDMS}} = 0.499$, $\nu_{\text{glass}} = 0.2$

4.1.4 Model parameters

The channel height and channel length were defined as 100 nm and 35.4 μm, respectively, in our model. The concentration of ionic solution was defined to achieve the desired EDL thickness in the low-concentration region. The interface region was defined as 1/100th the channel length. Applied voltage was varied to achieve a large range of induced pressures in the channel.

4.2 Deformation approximations

Previous work by Gervais shows that for a high-aspect-ratio rectangular channel ($w \gg h_0$) in a semi-infinite medium, the characteristic length scale of strain decay is simply proportional to the width of the channel (Gervais et al. 2006). Using this scaling argument, Gervais approximates the maximum deflection of the channel wall as

$$\delta = c\frac{pw}{E_{\text{mod}}} \tag{18}$$

where c is a proportionality constant of O (1). Here, we numerically verified the scaling argument for our system and numerically calculated the proportionality constant for given system parameters using COMSOL. Specifically, to model material deformation in our system, we consider a linear elastic isotropic material such that the stress–displacement relationship is given by

$$\boldsymbol{\sigma} = \frac{E_{\text{mod}}\,\nu}{(1-2\nu)(1+\nu)}\text{trace}(\boldsymbol{\epsilon}_{\boldsymbol{strain}})\boldsymbol{I} + \frac{E_{\text{mod}}}{1+\nu}\boldsymbol{\epsilon}_{\boldsymbol{strain}} \tag{19}$$

where $\boldsymbol{\sigma}$ is the stress tensor, E_{mod} is elastic modulus, ν is Poisson's ratio, $\boldsymbol{\epsilon}_{\boldsymbol{strain}}$ is the strain tensor, and $\boldsymbol{I}$ is the second-order identity matrix. We investigate two different geometric constraints typical in microfluidics: (a) a channel inside of a homogenous material (e.g., glass) where both walls deflect (Fig. 4b) and (b) a channel formed within a relatively soft material and bonded to a relatively stiff material (e.g., PDMS on glass) such that only one wall will deflect (Fig. 4c). In the case of a homogenous material, the boundary constraint on the system requires symmetry across the y-axis. In the second case, the boundary constraint requires that there is no deformation at the interface between the two materials. In either case, we define a boundary load p normal to the surface.

For our mesh, we used linear triangular elements with a higher mesh density defined in the region near the channel, as this is where the largest strain occurs. For the final

simulation results shown below, we used 53,000 to 58,000 elements and a channel height and width of 0.5 and 10 μm, respectively. Total substrate thickness and width were both defined as 1000 μm, and a pressure of 100 bar was applied.

Our model results show that for a sufficiently thick substrate thickness ($t/w \geq 10.9$) and high channel aspect ratio ($w/h_0 \geq 11.0$), the proportionality constant described by Eq. (18) holds within 1 % and does not depend on channel height, substrate thickness, or elastic modulus (see supplementary info, S1). Furthermore, simulations show that the proportionality constant c is different for the two cases and depends directly on Poisson's ratio (ν) (Fig. 4c). Finally, in Fig. 4d, we plot numerically determined dimensional values of deflection versus pressure for PDMS–glass and glass–glass channels with two different channel widths, with values that are comparable to those found in experimental conditions (Gervais et al. 2006; Hardy et al. 2009, data not shown).

4.3 Coupling flow model and deformation

Assuming that the channel length is much larger than the channel width such that the curvature along the width is much greater than the channel length, the deflection along the two directions are decoupled such that the deflection along the length of the channel depends only on the local pressure (van Honschoten et al. 2007) (see supplemental info, S2).

$$\delta(x) = c\frac{p(x)w}{E_{\text{mod}}} \tag{20}$$

Furthermore, assuming $w \gg h$ and $\delta \ll w$, the channel cross section can be closely approximated as rectangular as in previous work (Gervais et al. 2006; van Honschoten et al. 2007). In this situation, the hydraulic resistance in the channel is dependent only on the change in cross-sectional area and not on the shape of the channel (see supplementary info, S3). Thus, in order to couple deformation to our 2D flow model, we can simply adjust the channel height to the average deflection at each cross section. To do this, we define a coefficient that relates mean deflection to the maximum deflection at the center of the channel (Gervais et al. 2006, see S2). Interestingly, our simulations show that this coefficient has little dependence on geometry, pressures, and material properties and can be well assumed as 0.79 (±0.1 %). Therefore, the mean deformation using our model can be defined as:

$$\delta_{\text{mean}} = 0.79\, c\frac{p(x)w}{E_{\text{mod}}} \tag{21}$$

Given this mean deformation in the channel, we can, at each iteration, determine the maximum deflection (by dividing by the same coefficient) and determine whether we have channel collapse, or if another iteration is required for convergence.

5 Numerical results

In this section, we first determine the effect of EDL thickness on induced pressure. Next, we use our fully coupled flow/deformation model to calculate deformation in our system and examine the coupling between deformation and hydraulic resistance. Finally, we report examples of typical electrokinetic microfluidic systems that can deform and use our model to estimate maximum deformation after iteration and predict conditions of system failure.

5.1 COMSOL model with thick EDLs

To determine how EDL thickness effects pressure generation within a channel, we determined $\bar{p}$ for a range of conductivity ratios and relative EDL thicknesses for a single-electrolyte system and constant ζ-potential. Figure 5 shows our COMSOL results compared with analytical theory. In the limit of thin EDLs, our COMSOL model solution converges to the analytical solution (within 1 % deviation for relative EDL thickness of 0.01). Furthermore, we show that by increasing the relative EDL thickness, $\bar{p}$ is decreased. This phenomenon can be explained by the relationship between double layer thickness and net area averaged EOF velocity. In general, EOF velocity is uniform far from the wall, but will begin to decay in the EDL region. For thick EDLs, the region over which velocity decays is proportionally larger, and thus the mean velocity is reduced (Pennathur and Santiago 2005). Since the EDL thickness is, by definition, inversely proportional to the local concentration (Eq. 4), the EDL in the low-concentration region will be thicker than in the high-concentration region. This results in a smaller mismatch in EOF and thus lower induced pressure.

In order to quantify the effect of thick EDLs on resulting induced pressure, we plot the percent decrease in $\bar{p}$ as a function of relative EDL thickness, displaying conductivity ratio as error bars for each non-dimensional double layer thickness examined (Subplot Fig. 5). For relatively thick EDLs ($\lambda_D/h_0 = 0.5$), we show that pressure is decreased over 80 %, which can have a large mitigating effect on resultant deformation. In all cases, we note that the conductivity ratio is not as important as the EDL thickness when assessing the effect of the EDL thickness on resultant pressure. We have a performed a best fit to the data (over all conductivity values):

$$\%\,\text{decrease} = -241(\lambda_D/h_0)^2 + 296(\lambda_D/h_0) \tag{22}$$

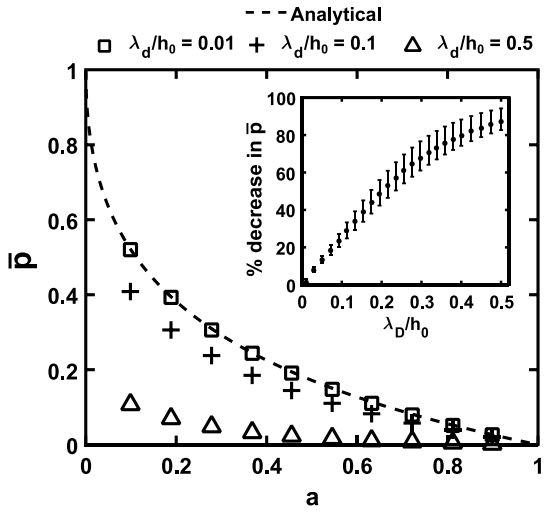

Fig. 5 Non-dimensionalized maximum pressure $\bar{p}$ for a given conductivity ratio and double layer thickness λ_D/h_0. Our numerical model is comparable with the analytical solution (*dotted line*) for the case of relatively thin double layers (*squares*). As the relative EDL thickness is increased, $\bar{p}$ decreases. (*inset*) Percent decrease in $\bar{p}$ from the analytical solution versus relative EDL thickness and conductivity ratio. This difference is maximized at thick EDLs and high-conductivity ratios (data not shown). *Error bars* show deviation from mean value over range of conductivity ratios. Lower limit is given by $a = 0.1$, and upper limit is given by $a = 0.9$. A second-order fit closely approximates this trend given by: $\%\,\text{decrease} = -241(\lambda_D/h_0)^2 + 296(\lambda_D/h_0)$

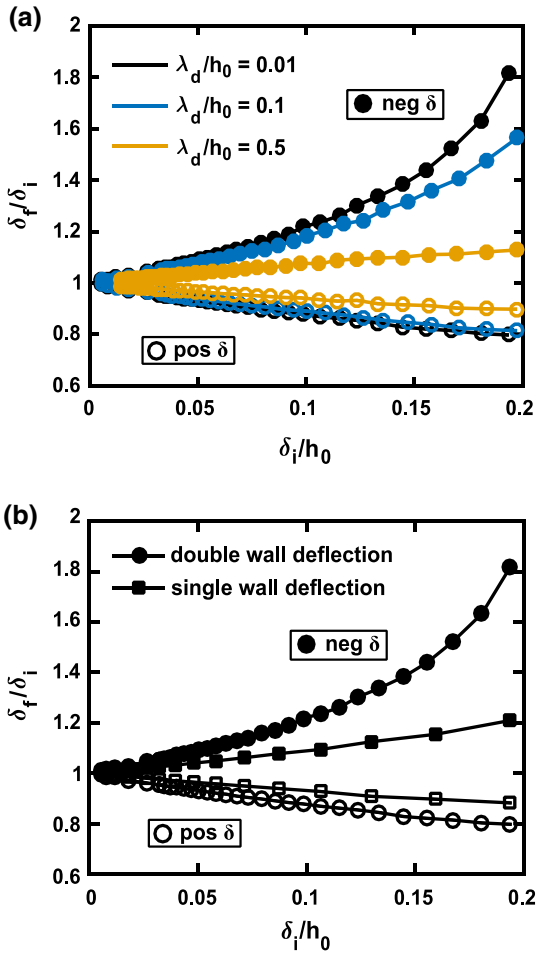

Fig. 6 **a** Relative final deflection (δ_f/δ_i) versus relative initial deflection (δ_i/h_0) in a glass channel for various EDL thicknesses (λ_D) and a conductivity ratio a of 0.1 calculated using our iterative COMSOL model. As EDL thickness increases, the effect of deflection decreases, implying that the EDLs aid in the suppression of deformation. Furthermore, we find that channel collapse is self-amplifying, while channel expansion is self-dampening. **b** Comparison of relative deflection values for both single-wall deflection (e.g., PDMS channel on glass) and double-wall deflection (e.g., channel in glass). Here, we only compare the results for thin EDL (λ_D/h_0) not only because PDMS channels are rarely small enough to experience double layer effects but also because the largest deflections are in thin EDLs systems. Results show that in the case of negative deflection (constriction) the iterative effects are reduced in the PDMS channel. Likewise, in the case of positive deflection (expansion), there is less dampening in the PDMS channel

which can be used to estimate the percent decrease in pressure due to specific EDL thicknesses. Furthermore, we note that the percent decrease in $\bar{p}$ is larger for conductivity ratios approaching 1 (data not shown, but larger conductivity ratios are the top of the error bars in the subplot of Fig. 4).

5.2 Deformation results

As previously mentioned, pressure in our proposed system is strongly dependent on the hydraulic resistance of the channel which is coupled with deformation. For example, in regions where the channel constricts, the local hydraulic resistance will increase, increasing the induced pressure gradient in the channel, and thus larger negative deformation. In order to better understand the general behavior of the coupling effects, we look at deformation calculations both prior and after coupling. We define the initial deformation δ_i as the channel deformation calculated prior to coupling (rigid channel), and final deformation δ_f as the deformation calculated with the fully coupled model.

Figure 6 shows the final channel wall deflection with respect to initial deflection (δ_f/δ_i) as a function of the relative initial deflection (δ_i/h_0) for different EDL thicknesses (Fig. 6a) and channel geometric constraints (Fig. 6b). We show that an iterative solution is especially necessary in cases where the initial deflection is large and negative. Positive deflection lessens the changes between initial and final deflection, and EDLs reduce this effect even further. The self-amplifying effect of channel collapse and self-dampening effect of channel expansion can be explained by considering how deformation affects the hydraulic resistance in the channel. In the case of channel collapse, the cross section of the channel is reduced and causes an increase in

Table 1 Example deflection calculations for typical micro-/nanofluidic system parameters

Material	a	λ_d/h_0	w (μm)	h_0	V	p_i (bar)	δ_i/h_0	p_f (bar)	δ_f/h_0
Glass	0.1	0.01	10	50 nm	−1500	−655	−0.17	−1038	−0.28
	0.1	0.1	10	50 nm	−1500	−517	−0.14	−667	−0.18
	0.1	0.5	10	50 nm	−1500	−133	−0.04	−137	−0.04
	0.5	0.01	10	50 nm	−1500	−216	−0.06	−238	−0.06
	0.9	0.01	10	50 nm	−1500	−33	−0.01	−34	−0.01
	0.1	0.01	10	50 nm	+1500	655	0.17	530	0.14
	0.1	0.01	10	30 nm	−1500	−1820	−0.81	X	X
PDMS	0.1	0.01	10	1 μm	−100	−0.11	−0.20	−0.13	−0.25
	0.1	0.01	10	1 μm	100	0.11	0.20	0.10	0.18

Here, we assume the following values for all calculations, $\zeta = 25\,\text{mV}$, $E_{\text{mod, PDMS}} = 0.4\,\text{MPa}$, $E_{\text{mod, glass}} = 72\,\text{GPa}$, $\epsilon_r = 79$, where ϵ_r is the relative permittivity of the fluid. The initial minimum pressure p_i is calculated using Fig. 5 and Eq. (10). Next, using Eq. (18) and the proportionality constant from Fig. 4c, we determine the initial deflection ratio (δ_i/h_0). Lastly, using this value along with Fig. 6, we determine the final equilibrium pressure p_f and resulting deflection δ_f. Here, total channel collapse is indicated by X

hydraulic resistance. When resistance is increased, a higher pressure gradient is required to maintain the same pressure-driven flow, leading to increased deformation. Eventually, these effects balance, and a convergence point is reached. Likewise, in the case of channel expansion, hydraulic resistance is decreased and a lower pressure gradient is required to balance the mismatch in EOF. As a result, we see that the induced deformation in this case is less than the initial prediction.

Next, in Fig. 6b, we compare: (a) a homogenous substrate where both walls deflect (e.g., glass) and (b) a channel formed in a soft material and bonded to a stiffer material such that only one wall deflects (e.g., PDMS on glass). Since the largest deformation occurs with thin EDLs, we only show those results here. As expected, the iterative effects on deformation are significantly reduced in the case of a single deflecting wall. This is due to the fact that changes in hydraulic resistance are halved for the same initial deflection, resulting in a lesser change in pressure gradients. For example, in a system with an initial relative deflection of 0.2, the final deflection will be 1.8X the initial deflection in the two deflecting wall system and only 1.2X for a single deflecting wall.

Note that the results shown in Fig. 6 were calculated for a conductivity ratio of 0.1. Our simulations show that the iterative behavior does not depend on conductivity ratio (see supplementary info, S6) and therefore indicates that the results shown in Fig. 6 can be generalized for all conductivity ratios.

Furthermore, constriction also changes the conductance in the channel since conductance is dependent on both the conductivity and channel geometry. Our COMSOL model takes into account the effect of geometry on conductance at each iteration, re-calcuating resulting conductance for each change in cross-sectional area. However, we do not take into account the change of conductivity (and therefore conductance) due to changing double layers, because in many systems, this effect is negligible (Pennathur and Santiago 2005) (see supplemental info, S5).

5.3 Example calculations for typical systems

Using the information from our COMSOL model, we are able to predict deformation behavior for typical micro- and nanofluidic systems. Specifically, we consider micro- and nanofluidic channels in both glass and PDMS and show deformation predictions in Table 1. To determine the values in Table 1, we use Fig. 5 and Eq. (10) to determine the initial maximum pressure, p_i, for a given channel geometry, applied potential V, and electrolyte properties. Next, the initial deflection is determined using Eq. (18) and the appropriate proportionality constant c from Fig. 4d. The final pressure and deformation is then determined using the data from Fig. 6.

Our results show that the resulting pressure and deformation in the channel is significantly decreased when EDL thickness in increased. For example, the resulting deformation in the glass channel (Table 1) decreases by 36 and 86 % when the relative EDL thickness is increased from 0.01 to 0.1 and 0.5, respectively. We further show that increasing the conductivity ratio significantly reduces the amount of deformation in the system. For example, increasing the conductivity ratio from 0.1 to 0.5 and 0.9 results in a 79 and 96 % decrease in pressure and deformation, respectively.

From our example calculations, we also noted that the direction in which the fluid is driven (toward region of high conductivity or low conductivity) can have a significant effect on the resulting deformation. For our glass channel example, when the applied voltage was reversed

(from −1500 V to +1500 V), the direction of deformation switches from negative to positive (collapse to expansion) and final deformation decreases by 50 %. Again in the PDMS channel example, reversing the polarity of the potential (from −100 V to +100 V) decreases the resulting deformation by 25 %. This large difference in deformation can be attributed to the effects of hydraulic resistance on deformation which were noted in Fig. 6; channel collapse increases hydraulic resistance and amplifies induced pressure, while channel expansion dampens the induced pressure.

Furthermore, we note that channel height has a significant effect on the pressures and deformation induced in the proposed channels. Decreasing the channel height from 50 to 30 nm results in a 178 % increase in magnitude of the initial pressure in the channel, causing full channel collapse. This large change can be attributed to the fact that pressure is inversely related to the square of the channel height (Eq. 8).

Finally, it is important to note that in all cases we use a model that has dispersion length between the two nonuniform regions that does not affect resultant solutions. However, the length of this interface can indeed affect the pressure predictions and has not been accounted for. In general, a large transition (dispersion) region will give values that approach analytical solution for thin EDLs, but as the length scale is decreased, pressure will increase due to an additional vertical pressure gradient. We predict that most influential factor is the relative difference between the dispersion length scale and the channel height. With smaller differences, our results will deviate more from experimental values. However, dispersion notwithstanding, we believe that our results should be within error with typical microfluidic systems, since errors will only be exacerbated in rarely found disperse nanoscale systems.

6 Conclusion

In this work, we used both an analytical and COMSOL numerical model to study induced pressures and subsequent deflection in electrokinetic microfluidic systems. Specifically, we calculate the pressures in electrokinetic systems with step changes in conductivity and/or ζ-potential, for both thin and thick EDLs. These induced pressures are shown to be significant enough to induce large deformation in channels. To solve for the deformation in the channel, we use a scaling approximation to relate pressure and deflection in two well-known microfluidic materials. This scaling approximation is coupled with our electrokinetic model to solve iteratively for the final deflection given an electrokinetic system with various parameters. When applying this model to real-world scenarios, we find that channel collapse can occur in channels with large electric fields, small channel heights, and large channel widths and is especially exacerbated for soft materials such as PDMS. This study not only shows that deformation is an important consideration in micro- and nanofluidic electrokinetic systems with step changes in conductivity and/or ζ-potential, but also allows one to quickly determine whether deflection should be considered in their particular system. This model and resulting data thus has huge implications in applications such as nanofluidic electrocavitation, ITP at the micro- and nanoscale, and FASS.

Acknowledgments This work was supported by the US Army Research Office under cooperative agreement W911NF-12-1-0031, and Institute for Collaborative Biotechnologies through grant W911NF-09-0001 from the US Army Research Office. The content of the information does not necessarily reflect the position or the policy of the Government, and no official endorsement should be inferred. The authors also acknowledge Peter de Rutte for his help with the literature search.

References

Abgrall P, Nguyen NM (2008) Nanofluidic devices and their applications. Anal Chem 80:2326–2341. doi:10.1021/ac702296u

Bharadwaj R, Santiago JG (2005) Dynamics of field-amplified sample stacking. J Fluid Mech 543:57. doi:10.1017/s0022112005005975

Bruin GJM (2000) Recent developments in electrokinetically driven analysis on microfabricated devices. Electrophoresis 21:3931–3951. doi:10.1002/1522-2683(200012)21:18<3931:AID-ELPS3931>3.0.CO;2-M

Dendukuri D, Gu SS, Pregibon DC, Hatton TA, Doyle PS (2007) Stop-flow lithography in a microfluidic device. Lab Chip 7:818–828. doi:10.1039/B703457A

Gervais T, El-Ali J, Gunther A, Jensen KF (2006) Flow-indeuced deformation of shallow microfluidic channels. Lab Chip 6:500–507. doi:10.1039/B513524A

Gillespie D (2015) A review of steric interactions of ions: why some theories succeed and others fail to account for ion size. Microfluid Nanofluid 18:717–738. doi:10.1007/s10404-014-1489-5

Hardy BS, Uechi K, Zhen J, Pirouz KH (2009) The deformation of flexible PDMS microchannels under a pressure driven flow. Lab Chip 9:935–938. doi:10.1039/B813061B

Herr AE, Molho JI, Santiago JG, Mungal MG, Kenny TW, Garguiloae MG (2000) Electroosmotic capillary flow with nonuniform zeta potential. Anal Chem 72:1053–1057. doi:10.1021/ac990489i

Hosokawa K, Hanada K, Maeda R (2001) A polydimethylsiloxane (PDMS) deformable diffraction grating for monitoring of local pressure in microfluidic devices. J Micromech Microeng 12(1):1

Hunter RJ (1981) Zeta potential in colloidal science: principles and applications. Academic press, San Diego, CA

Janssen KGH, Pennathur S (2015) Electrocavitation in nanofluidics: unique phenomenon and fundamental platform. Lab Chip 15:3980–3983. doi:10.1039/C5LC00692A

Janssen KGH, Eijkel JCT, Tas NR, de Vreede LJ, Hankemeier T, van der Linden HJ (2011) Electrocavitation in nanochannels. In: Proceedings MicroTAS, W2E. Seattle WA, USA

Lenzi A, Viola F, Bonotto F, Frey J, Napoli M, Pennathur S (2011) Method to determine the effective zeta potential in a microchannel with an embedded gate electrode. Electrophoresis 32:3295–3304

Loessberg-Zahl J, Janssen KGH, McCallum C, Gillespie D, Pennathur S (2016) (Almost) stationary isotachophoretic concentration boundary in a nanofluidic channel using charge inversion. Anal Chem. doi:10.1021/acs.analchem.6b01701

Majumder A, Tiwari AK, Korada K, Ghatak A (2010) Microchannel induced surface bulging of a soft elastomeric layer. J Adhes Sci Technol 24:2681–2692

Mijatovic D, Eijkel JCT, van den Berg A (2005) Technologies for nanofluidic systems: top-down vs. bottom-up-a review. Lab Chip 5:492–500. doi:10.1039/B416951D

Pennathur S (2001) Microscale turbopump cavitation. M.S. Thesis, Department of Aeronautics and Aerospace, MIT

Pennathur S, Santiago JG (2005) Electrokinetic transport in nanochannels: 2. Experiments. Anal Chem 77:6782–6789

Quake SR, Scherer A (2000) From micro- to nanofabrication with soft materials. Science 290:1536–1540. doi:10.1126/science.290.5496.1536

Sadr R, Yoda M, Zheng Z, Conlisk AT (2004) An experimental study of electro-osmotic flow in rectangular microchannels. J Fluid Mech 506:357–367

Squires TM, Quake SR (2005) Microfluidics: fluid physics at the nanoliter scale. Rev Mod Phys 77:977. doi:10.1103/RevModPhys.77.977

Unger MA, Chou HP, Thorsen T, Schherer A, Quake SR (2000) Monolithic microfabricated valves and pumps by multilayer soft lithography. Science 288:113–116

van Honschoten JW, Escalante M, Tas NR, Jansen HV, Elwenspoek M (2007) Elastocapillary filling of deformable nanochannels. J Appl Phys 101:094310

van Schoot DS, Janssen KG, Tas NR, Hankemeier T, Eijkel JCT (2014) Electrocavitation in nanochannels. In: Mercury L, Tas N, Zilberbrand M (eds) Transport and reactivity of solutions in confined hydrosystems. Springer, pp 141–150

Wainright A, Williams SJ, Ciambrone G, Xue Q, Wei J, Harris D (2002) Sample pre-concentration by isotachophoresis in microfluidic devices. J Chromatogr A 979:69–80

Xia Y, Whitesides GM (1998) Soft lithography. Annu Rev Mater Sci 28:153–184